A coupled-channel model of the 3 u states of N 2 : Structure and interactions of the 3 s g F 3 3 u and 3 p u G 3 3 u Rydberg states

B. R. Lewis, A. N. Heays, S. T. Gibson, H. Lefebvre-Brion, and R. Lefebvre

Citation: The Journal of Chemical Physics **129**, 164306 (2008); doi: 10.1063/1.2990656
View online: http://dx.doi.org/10.1063/1.2990656
View Table of Contents: http://scitation.aip.org/content/aip/journal/jcp/129/16?ver=pdfcov
Published by the AIP Publishing

A coupled-channel model of the $^3\Pi_u$ states of N_2: Structure and interactions of the $3s\sigma_g F_3\ ^3\Pi_u$ and $3p\pi_u G_3\ ^3\Pi_u$ Rydberg states

B. R. Lewis,[1,a)] A. N. Heays,[1] S. T. Gibson,[1] H. Lefebvre-Brion, and R. Lefebvre
[1]*Research School of Physical Sciences and Engineering, The Australian National University, Canberra, Australian Capital Territory 0200, Australia*
[2]*Laboratoire de Photophysique Moléculaire, Bâtiment 213, Université de Paris-Sud, 91405 Orsay Cedex, France*

(Received 23 June 2008; accepted 4 September 2008; published online 24 October 2008)

New and existing spectroscopic data on N_2, obtained using a wide variety of experimental techniques, are interpreted using a coupled-channel Schrödinger-equation (CSE) model of the structure and predissociation dynamics for the interacting Rydberg and valence states of $^3\Pi_u$ symmetry. As a result, $v>0$ levels of the $3p\pi_u G_3\ ^3\Pi_u$ Rydberg state are assigned correctly for the first time, leading to the identification of very strong perturbations in the G_3-state vibrational structure. A four-channel CSE model, which includes the $3s\sigma_g F_3\ ^3\Pi_u$ and $3p\pi_u G_3\ ^3\Pi_u$ Rydberg states and the $C'\ ^3\Pi_u$ and $C\ ^3\Pi_u$ valence states, indicates strong Rydberg–Rydberg coupling between the F_3 and G_3 states, strong Rydberg-valence coupling between the G_3 and C' states, and weaker coupling between the F_3 and C' states. © *2008 American Institute of Physics*.
[DOI: 10.1063/1.2990656]

I. INTRODUCTION

Knowledge of molecular-nitrogen spectroscopy and dissociation dynamics in the extreme ultraviolet (EUV) region is essential for a proper understanding of the radiative and photochemical processes occurring in nitrogen-rich planetary atmospheres. In particular, the correct interpretation of data from the Cassini–Huygens encounter with the Saturnian moon, Titan, relies on such knowledge, as demonstrated recently in a study tracing the source of the N-isotope anomaly in Titanic HCN.[1]

It has been confirmed recently, in a coupled-channel Schrödinger-equation (CSE) study,[2] that the $^1\Pi_u$ states of N_2 excited in the lowest dipole-allowed transitions, albeit in the EUV, predissociate by spin-orbit coupling to the $^3\Pi_u$ manifold. However, that study[2] considered only the $C\ ^3\Pi_u$ and $C'\ ^3\Pi_u$ valence states and was limited to excitation energies below $\sim 105\,000\ \mathrm{cm}^{-1}$, a region largely uninfluenced by interactions involving the $3s\sigma_g F_3\ ^3\Pi_u$ and $3p\pi_u G_3\ ^3\Pi_u$ Rydberg states. Hereafter, for brevity, we will refer to these states as F and G, respectively.

Until recently, the only available experimental data on the F and G states had been derived from low-resolution electron energy-loss[3–7] and translational[8] spectroscopy, with vibrational assignments uncertain. In the preceding companion paper in this issue,[9] the experimental database on the $^3\Pi_u$ states of N_2 has been reviewed, and significant new optical data are presented on the $F(v=0,1)$ and $G(v=0,1)$ levels, and the $C(v\geq 7)$-state levels above $100\,000\ \mathrm{cm}^{-1}$. Additional high-resolution optical studies of the $F(v=0)$ (Ref. 10) and $G(v=0)$ (Ref. 11) levels, which have been performed very recently, suggest a strong degree of interaction between the F and G states.

Numerical potential-energy curves for the $^3\Pi_u$ states of N_2 are not readily available, but accurate multireference configuration-interaction calculations of the lowest four adiabatic valence states of that symmetry have been performed by Guberman,[12] Dateo,[13] and Partridge,[14] the latter of which are shown in Fig. 1, together with schematic F- and G-state potentials.[15] No comprehensive *ab initio* calculations of the type performed by Spelsberg and Meyer[16] for the $^1\Pi_u$ and $^1\Sigma_u^+$ states of N_2, which include both the Rydberg and valence states, together with their interactions, are available for the $^3\Pi_u$ states.

In the present work, a semiempirical CSE model of the spectroscopy and predissociation dynamics of the coupled Rydberg and valence $^3\Pi_u$ states of N_2 is developed, guided principally by the new experimental information in the companion paper[9] and Refs. 10 and 11. The model confirms a strong interaction between the F and G Rydberg states, which is presumably responsible for the previously incorrect,[3,4,6,7] or missing,[5,8] vibrational assignments for the $G(v\geq 1)$ levels. The inclusion of the F and G states in the $^3\Pi_u$ model should enable the extension of the $^1\Pi_u$ predissociation model of Lewis *et al.*[2] to higher transition energies.

II. COUPLED-CHANNEL MODEL

A. Techniques

Two different coupled-channel methods are employed to treat the $^3\Pi_u$ states of N_2 and their interactions, the first of which is the CSE technique[17] used previously in our study of the $^1\Pi_u$ predissociation mechanisms in N_2.[2] A similar application of the CSE technique for the case of O_2 has been described in detail in Ref. 18. Briefly, the diabatic-basis coupled-channel radial Schrödinger equation for the coupled $^3\Pi_u$ states is solved numerically to yield the coupled-channel wave function for the excited state, which is then combined

a)Electronic mail: brenton.lewis@anu.edu.au.

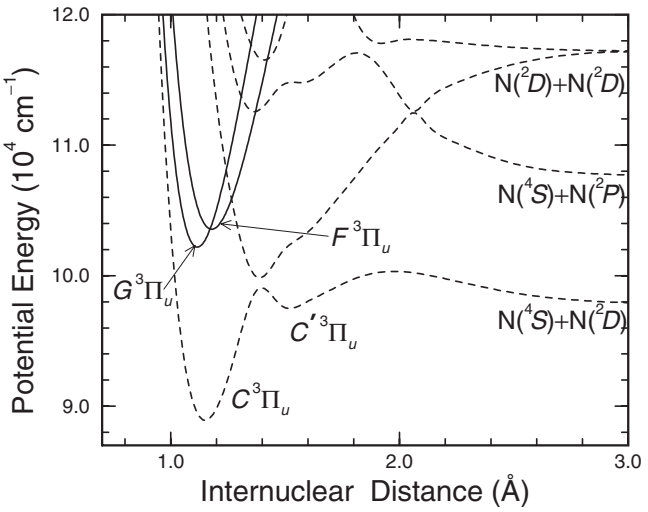

FIG. 1. The $^3\Pi_u$ potential-energy curve manifold of N_2. Dashed curves: the *ab initio* (adiabatic) valence potentials of Partridge (Ref. 14) calculated at the multireference configuration-interaction plus Davidson correction level. Solid curves: schematic potentials for the *F* and *G* Rydberg states, shown in a diabatic (crossing) representation. The energy scale is referenced to the $v=0$, $J=0$ level of the $X\,^1\Sigma_g^+$ ground state (not shown). The lowest dissociation limit, $N(^4S)+N(^4S)$ at ~78 710 cm^{-1}, is beyond the scale of the figure.

with the ground-state radial wave function and nominal diabatic electronic transition moments, to form a total "photodissociation cross section."[19] Transition energies and predissociation linewidths, derived from the computed cross section through the least-squares fitting of Beutler–Fano profiles, are then compared with experimental results iteratively in order to optimize the relevant CSE-model parameters, i.e., the potential matrix $\mathbf{V}(R)$, where R is the internuclear distance, which contains the diabatic triplet potential-energy curves (diagonal elements) and couplings (cross terms). Isotopic calculations are performed simply by changing the value of the reduced molecular mass in the CSE model, while rotational calculations are performed by including an appropriate centrifugal term in the Hamiltonian.

In the second method, complex resonance energies E_r are calculated for the coupled $^3\Pi_u$ states using a coupled-channel code with matching of inward and outward solutions, the resonance widths given by $-2\,\mathrm{Im}(E_r)$. An external complex scaling[20] of the coordinate in the asymptotic region of all potentials and couplings allows the use of the same boundary conditions for resonances and bound states.[21] This additional method is able to provide mixing coefficients for the strongly coupled levels, which are not available readily using the CSE method. In most cases, specifically for relatively isolated resonances, both computational methods give identical results for the resonance energies and widths. However, in the few cases of very broad interacting resonances, there are small differences and uncertainties, generally $\lesssim$15% of the relevant resonance width.

B. Electrostatic interactions

The diabatic-basis $^3\Pi_u$ electronic states of N_2 used in the CSE model are associated primarily with the following molecular-orbital (MO) configurations:

$$G\,^3\Pi_u: \cdots (2\sigma_u)^2(3\sigma_g)(1\pi_u)^4 3p\pi_u, \quad (1)$$

$$F\,^3\Pi_u: \cdots (2\sigma_u)^2(3\sigma_g)^2(1\pi_u)^3 3s\sigma_g, \quad (2)$$

$$C\,^3\Pi_u: \cdots (2\sigma_u)(3\sigma_g)^2(1\pi_u)^4(1\pi_g), \quad (3)$$

$$C\,^3\Pi_u, C'\,^3\Pi_u: \cdots (2\sigma_u)^2(3\sigma_g)(1\pi_u)^3(1\pi_g)^2, \quad (4)$$

where $\cdots$ represents the $(1\sigma_g)^2(1\sigma_u)^2(2\sigma_g)^2$ occupancies common to all of the MOs. The *G* state is the lowest member of the $np\pi_u$ Rydberg series, converging on the $X\,^2\Sigma_g^+$ ground state of the molecular ion, while the *F* state is the lowest member of the $ns\sigma_g$ Rydberg series, converging on the $A\,^2\Pi_u$ first-excited state. The MO configuration (4) gives rise to four $^3\Pi_u$ states.[22] The *C* state has an unusually shaped potential-energy curve (see Fig. 1), displaying a marked change from the valence-hole configuration (3) to the valence configuration (4), as *R* increases through 1.3–1.4 Å.[23] In the region $R\approx 1.5$ Å, the C' and *C* states can be thought of as the lowest two $^3\Pi_u$ states associated principally with MO configuration (4). All combinations of the MO configurations (1)–(4) differ in exactly two of the occupied electron orbitals, leading to the possibility of strong electrostatic interactions between the associated electronic states of like symmetry,[24] already demonstrated in the case of the isoconfigurational $^1\Pi_u$ states,[2,16,25] including Rydberg-valence, Rydberg–Rydberg, and valence-valence interactions. Indeed, the interactions between configurations (3) and (4) are already apparent in the shape of the *C*-state potential in Fig. 1. The remaining interactions between our adopted diabatic-basis states are considered explicitly in what follows.

C. Experimental database

The experimental data used here to optimize the CSE model for the interacting $^3\Pi_u$ states were drawn from a variety of sources, with isotopic measurements included wherever possible. Level energies for $C(v=0-4)$ were deduced from the C-$X(v,0)$ origins of Dieke and Heath,[26] as revised by Tilford *et al.*,[27] while the C-$B(v,v'')$ rotational analyses of Roux *et al.*[28] were employed for the corresponding rotational constants. Spectroscopic parameters for the $C(v=5)$ and $C'(v=0-2)$ levels were taken from the studies of Ledbetter,[29] Carroll,[30] Ledbetter and Dressler,[31] and Tanaka and Jursa,[32] while those for the Rydberg $F(v=0)$ and $G(v=0)$ levels were based on the recent high-resolution studies of Sprengers *et al.*[10] and Hashimoto and Kanamori, respectively.[11] For the higher vibrational levels of the *C* state, i.e., $C(v=7,8,16,18)$ for $^{14}N_2$, and $C(v=7,13,14)$ for $^{15}N_2$, and also the $G(v=1)$ level of $^{14}N_2$ and the $F(v=1)$ levels of $^{14}N_2$ and $^{15}N_2$, the new data from the preceding companion paper were employed, including predissociation linewidths.[9] Finally, level energies adapted from the low-resolution translational-spectroscopic study of van der Kamp *et al.*[8] were used for the higher Rydberg levels $F(v=2,3)$ and $G(v=2,3)$.[33] These adopted experimental data are summarized in columns 3, 7, and 10 of Table I.

Since we have drawn on a wide range of data, accumulated over many years using various experimental techniques, with rotationally resolved results originally analyzed

TABLE I. Comparison between experimental and fitted CSE-model spectroscopic parameters and predissociation widths for the $^3\Pi_u$ levels of N_2.

Isotopomer	Level	T_{exp} [a]	Refs.	T_{CSE} [a]	ΔT [a]	B_{exp} [b]	B_{CSE} [b]	ΔB [b]	Γ_{exp} [c]	Γ_{CSE} [c]
$^{14}N_2$	$C(0)$	88 980.0	27 and 28	88 980.1	−0.1	1.815	1.815	0.000		0.000
	$C(1)$	90 974.4	27 and 28	90 974.2	0.2	1.793	1.793	0.000		0.000
	$C(2)$	92 915.1	27 and 28	92 915.3	−0.2	1.769	1.769	0.000		0.000
	$C(3)$	94 789.1	27 and 28	94 788.9	0.2	1.740	1.740	0.000		0.000
	$C(4)$	96 570.3	27 and 28	96 570.2	0.1	1.701	1.701	0.000		0.000
	$C'(0)$	97 563.7	30	97 563.7	0.0	1.049	1.049	0.000		0.000
	$C(5)$	98 133.	29	98 133.	0.	1.407	1.407	0.000		0.000
	$C'(1)$	98 359.7	31	98 359.9	−0.2	1.218	1.218	0.000		0.000
	$C'(2)$	98 943.(5)	32	98 944.	−1.		1.028			0.000
	$C(7)$	101 069.(2)	9	101 069.	0.	1.38(2)	1.41	−0.03	16.(3)	15.
	$C(8)$	102 054.(3)	9	102 052.	2.		1.30		18.(4)	17.
	$G(0)$	103 317.4	11	103 317.4	0.0	1.885	1.884	0.001	0.11(1)[d]	0.09
	$F(0)$	104 730.6(1)	10	104 730.6	0.0	1.805(1)	1.806	−0.001	0.45(3)	0.46
	$G(1)$	106 167.(1)	9	106 167.	0.		1.839		9.6 (12)	9.6
	$F(1)$	106 579.(2)	9	106 579.	0.	1.75(3)	1.75	0.00	16.(3)	16.
	$G(2)$	108 030.(50)	8	108 032	−2		1.78			89.
	$C(16)$	108 293.(3)	9	108 293.0	0.0	1.153(2)	1.154	−0.001	≲0.5	0.01
	$C(18)$	109 727.(6)	9	109 724.	3.	1.08(2)	1.10	−0.02	5.0(17)	4.0
	$F(2)$	108 640.(50)	8	108 649	−9		1.70			148.
	$F(3)$	109 980.(50)	8	109 972	8		1.73			138.
	$G(3)$	110 800.(80)	8	110 831	−31		1.8			254.
$^{15}N_2$	$C(7)$	100 893.(2)	9	100 892.	1.	1.31(2)	1.33	−0.02	15.(3)	13.
	$C(13)$	105 727.(3)	9	105 728.	−1.	1.11(2)	1.11	0.00	2.3(13)[e]	1.6
	$C(14)$	106 477.3(3)	9	106 478.3	−1.0	1.12(1)	1.14	−0.02	~0.05 [f]	0.02
	$F(1)$	106 537.(3)	9	106 538.	−1.	1.61(4)	1.58	0.03	18.(2)	16.

[a] T_{v0} in cm^{-1}. $\Delta T = T_{exp} - T_{CSE}$.
[b] Effective e-level rotational constant for $J \leq 5$ in cm^{-1}. $\Delta B = B_{exp} - B_{CSE}$.
[c] Low-J predissociation width in cm^{-1} FWHM.
[d] Estimated value for $J \approx 11$, from Fig. 2 of Ref. 11.
[e] Width for $J \approx 13$.
[f] Estimated value for $\Omega = 2$, $J \approx 4$.

using several different $^3\Pi$ Hamiltonians, for database consistency we have endeavored to reference all energy data presented in Table I to the $^3\Pi$ Hamilton of Brown and Merer[34] that has been employed in Ref. 9. In Table I, the vibronic energies T_{exp} refer to the corresponding *deperturbed*, extrapolated F_2 ($\Omega = 1$, $J = 0$) triplet sublevel, the rotational constants B_{exp} are *effective* e-parity values over the range $J = 0-5$, and, as far as is possible, the predissociation linewidths Γ_{exp} represent low-J values.

D. Model fitting

The main goal of this work is to study the broad structure and electronic interactions of the $^3\Pi_u$ manifold of N_2. Therefore, a simple four-state CSE model has been adopted in which the C, C', F, and G states are treated as singlets [$\Omega = 1$ (F_2) levels only], with internal spin structure and spin-orbit and rotational interactions with other electronic states ignored. This model requires a compatible experimental database to be used in the iterative comparison with the CSE-model calculations, leading to the particular choice of experimental parameters in Table I. Specifically, the vibronic energies employed are independent of the effects of the triplet structure, while the e-parity effective rotational constants are independent of the very significant perturbation of the $G\,^3\Pi_{1u}$-state f-parity levels caused by first-order **L**-uncoupling interaction with the $D\,^3\Sigma^+_{0u}$ state, which is a member of the same Rydberg $3p$-complex.[24] Finally, the use of low-J predissociation linewidths allows rotational predissociation, the coupling terms for which are not included in the model, to be ignored.

The parameters of the four-state CSE model, specifically the potential-energy curves and electrostatic couplings, were varied in a controlled fashion during an iterative least-squares optimization procedure against the experimental database of Table I, including vibronic energies, rotational constants, and predissociation linewidths, for both $^{14}N_2$ and $^{15}N_2$. Initial potential-energy curves for the C and C' valence states were taken from Ref. 2. Initial curves for the F and G Rydberg states were obtained by energy shifting those for the isoconfigurational $o\,^1\Pi_u$ and $c\,^1\Pi_u$ states, also taken from Ref. 2. During the first stages of optimization, the curves were allowed to shift and/or be linearly scaled in the X and Y directions. In the final stages, further improvements were possible, in the case of the bound portions of the C and C' states, by allowing points on the curves to vary independently, while the inner and outer limbs were constrained with only smooth adjustments. The electrostatic coupling parameters were taken to be R-independent since it was not possible to determine any statistically significant R-dependence during the fitting procedure. The process of iteration was not

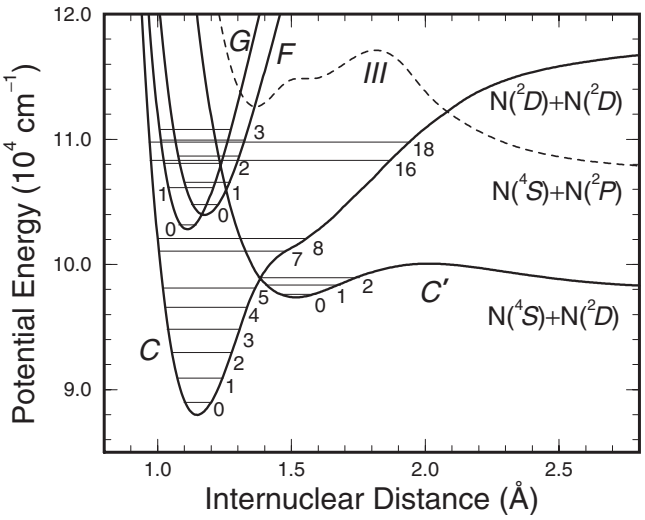

FIG. 2. Diabatic-basis potential-energy curves for the $^3\Pi_u$ states of N_2 (solid curves), determined by fitting CSE-model calculations to the experimental database. Coupled-channel energies for the observed levels of $^{14}N_2$ are indicated (horizontal lines), located in the potential curve corresponding to their principal electronic character. The lowest of the higher-energy $^3\Pi_u$ valence states, not included in the model, is also shown (dashed curve, labeled III, after Ref. 14). The energy scale zero reference is defined in the caption of Fig. 1.

completely straightforward, largely due to the restricted experimental database which includes a wide range of data, from the very precise to the very uncertain. Satisfactory results were possible only after careful attention was paid to the relative weights of the various experimental data included in the least-squares fitting process.

III. RESULTS AND DISCUSSION

A. Model parameters

The final diabatic-model potential-energy curves resulting from the fitting procedure are shown as the solid curves in Fig. 2.[35] In order to emphasize the range of applicability of the present model, a potential-energy curve is also shown (dashed curve) for the next-lowest $^3\Pi_u$ valence state, labeled III, which is adapted from the *ab initio* calculations of Partridge[14] (see Fig. 1). The outer limb of this potential, shown in a diabatic representation, crosses that of the C state in the 112 000 cm^{-1} region, while the inner part of the potential crosses the F- and G-state curves at only slightly higher energies. The $C \sim$ III interaction is expected to be fairly weak, as demonstrated by the small minimum splitting between the corresponding adiabatic potentials calculated by Partridge[14] (see Fig. 1) and Guberman,[12] in the region of their avoided crossing, but will affect predissociation patterns and branching ratios.[12] An estimate of ~200 cm^{-1} for the $G \sim$ III electrostatic coupling can be obtained from the 0.002 eV electron-capture width for the III state computed *ab initio* by Guberman[12] for $R=2.0$ a.u. in his theoretical study of the dissociative recombination (DR) of ground-state N_2^+, on which core the Rydberg G state is built.[36] The $F \sim$ III interaction is unknown, but may well be stronger, affecting the corresponding Rydberg-state energy-level structure and predissociation pattern in this region. Since all of these effects are neglected in the present CSE model, which does not include the diabatic III state, it is not expected that the model results will necessarily be valid in the $v \gtrsim 3$ region of the Rydberg states and the $v \gtrsim 19$ region of the C valence state.

TABLE II. Spectroscopic parameters determined for the present diabatic-model $^3\Pi_u$ Rydberg-state potential-energy curves, compared with those for the isoconfigurational $^1\Pi_u$ potentials (Ref. 2) and the corresponding limiting ionic states (Ref. 37). Values in parentheses are 1σ uncertainties returned by the fitting procedure, in units of the last significant figure.

State	T_e (cm^{-1})	R_e (Å)	ω_e (cm^{-1})	ΔT_e (cm^{-1}) [a]
$3p\pi_u\ G\ ^3\Pi_u$	104 000(20)	1.113(5)	2170(10)	
$3p\pi_u\ c\ ^1\Pi_u$	104 593	1.113	2234	593
$N_2^+\ X\ ^2\Sigma_g^+$		1.116	2207	
$3s\sigma_g F\ ^3\Pi_u$	105 132(20)	1.176(5)	1909(10)	
$3s\sigma_g\ o\ ^1\Pi_u$	105 976	1.175	1906	844
$N_2^+\ A\ ^2\Pi_u$		1.175	1904	

[a] $T_e(^1\Pi_u) - T_e(^3\Pi_u)$ for isoconfigurational states.

The diabatic-model potentials for the valence states differ only marginally from those of Ref. 2, having better-defined limbs for the C (inner and outer) and C' (inner) states due to the more extensive experimental database used in the fitting procedure. They also differ systematically from those deduced from the *ab initio* curves of Partridge,[14] shown in Fig. 1, by relatively small amounts, as discussed in more detail in Ref. 2. Spectroscopic parameters determined for the Rydberg $F\ ^3\Pi_u$- and $G\ ^3\Pi_u$-state diabatic-model potentials, given in Table II, are in good agreement with those for the isoconfigurational singlet states, $o\ ^1\Pi_u$ and $c\ ^1\Pi_u$, respectively, and also with those for the corresponding limiting ionic potentials, $N_2^+\ A\ ^2\Pi_u$ and $X\ ^2\Sigma_g^+$, respectively. As can be seen in Table II, the fitted o-F singlet-triplet splitting exceeds the c-G splitting, as predicted by the *ab initio* calculations of both Lefebvre-Brion and Moser[38] and Cremaschi *et al.*[39]

The full (symmetric) potential matrix deduced by means of the fitting process is

$$\mathbf{V}(R) = \begin{pmatrix} V_C(R) & 798(15) & \cdots & \cdots \\ 798(15) & V_{C'}(R) & 315(60) & 1175(200) \\ \cdots & 315(60) & V_F(R) & 1115(15) \\ \cdots & 1175(200) & 1115(15) & V_G(R) \end{pmatrix}, \tag{5}$$

where the diagonal elements correspond to the diabatic-basis potentials just discussed, and the off-diagonal elements, in cm^{-1}, with fitting uncertainties also shown, represent the coupling matrix elements within the $^3\Pi_u$ manifold. While it is not possible to determine the sign of an individual off-diagonal matrix element, the least-squares procedure has established definitively, through fitting the F- and G-state level widths, that the sign of the product of the three couplings $V_{C'F}V_{FG}V_{GC'}$ is *positive*.

The coupling $V_{CC'}$ is responsible primarily for the perturbation of the C- and C'-state vibrational levels, together with the predissociation of the higher C-state levels, in association with the crossing of their potentials near $R=1.39$ Å (see Fig. 2). Because of the aforementioned strong configurational change in the C state in this region, it can be ex-

pected that couplings involving this state will be *R*-dependent. However, since the *C*- and *C'*-state curves cross, it is the value of $V_{CC'}$ at the crossing point that is the important factor in their mutual perturbation.[24] Thus, the assumption of no *R*-dependence does not limit the analysis, the fitting procedure simply returning the value at the crossing point, $V_{CC'}=798(15)$ cm^{-1}, which agrees within the combined uncertainties with our previous value of 810(20) cm^{-1},[2] and also with the most recent *ab initio* value of 770 cm^{-1} (Refs. 2 and 40), but lies somewhat above the only other semiempirical estimate of ~700 cm^{-1},[31] which was based on a less complete experimental database.

The CSE fitting analysis also returns a robust value of $V_{FG}=1115(15)$ cm^{-1}, indicating a strong interaction between the *F* and *G* Rydberg states, whose series converge on different electronic states of the N_2^+ ion. This is one of the important results of this work, supporting the conclusions in two recent experimental papers regarding the mixing of the $F(v=0)$ and $G(v=0)$ levels.[10,11] It is the V_{FG} coupling that is responsible primarily for the extreme perturbation of the *G*-, and, to a lesser extent, *F*-state vibrational levels. It is this perturbation that has resulted in the lack of correct assignments for the $G(v>0)$ levels until now. The strength of the $F\sim G$ interaction should not be surprising: based on the work of Spelsberg and Meyer[16] and Lewis *et al.*,[2] the isoconfigurational singlet states exhibit a coupling of $V_{oc}\approx 800$ cm^{-1} near $R=1.12$ Å.

Because of the strong $F\sim G$ coupling, the additional coupling of the repulsive inner limb of the *C'* state to each Rydberg state influences the *F*- and *G*-state predissociation patterns in a complex manner with quantum-interference effects operative. There are significant uncertainties in each of the returned couplings, $V_{FC'}=315(60)$ cm^{-1} and $V_{GC'}=1175(200)$ cm^{-1}, reflecting not only the relative paucity of experimental predissociation linewidth data on the Rydberg vibrational levels but also some degree of coupling between these parameters in the fitting process. In fact, the *ratio* of these two couplings is somewhat better defined than the individual uncertainties would indicate. It is clear from the analysis that at least a three-state interaction is necessary to explain simultaneously the significant predissociation level widths for $G(v=0)$ and $F(v=0)$.[41] Furthermore, the ratio of these widths varies strongly as the ratio of the two couplings is changed. Our value for $V_{GC'}$ is somewhat lower than the value of ~1700 cm^{-1} estimated from the corresponding ~0.12 eV electron-capture width calculated by Guberman.[36,42] The difference is probably explicable by noting that the present and DR studies sample different regions of internuclear distance: the relevant diabatic curve crossings are at smaller *R* for the DR process (ionic ground-state crossing) than for the present work where the valence state crosses the much lower-energy Rydberg state at a significantly larger *R* value. In general, the couplings decrease significantly as *R* increases through this region (see, e.g., Ref. 16, for the singlet-state picture).

The lack of entries for the $C\sim F$ and $C\sim G$ couplings in Eq. (5) implies only that it was impossible to determine these parameters in the fitting procedure with any statistical significance since there appeared to be no corresponding sensitivity in any of the fitted quantities. Therefore, V_{CF} and V_{CG} were set to zero in the model calculations. However, in reality, these couplings may be strong: in the case of the isoconfigurational $^1\Pi_u$ states, the analogous couplings are $V_{bo}\approx 300$ cm^{-1} and $V_{bc}\approx 900$ cm^{-1}, respectively, at $R=1.12$ Å.[2,16] Furthermore, a value of ~1200 cm^{-1} can be estimated for V_{CG} from the corresponding 0.063 eV electron-capture width of Guberman[36,42] (but note remarks on *R*-dependence, above). The uncertainty regarding the values of these $^3\Pi_u$ couplings need not be of concern. Since the *C* state lies well below the *F* and *G* states, the principal effect of coupling between them will be to push the Rydberg states to higher energies, by about 70 cm^{-1}, e.g., if the relevant electrostatic coupling is as large as 1000 cm^{-1}. Therefore, in order to fit the experimental database, each particular choice of V_{CF} and V_{CG} will result in a slightly different set of diabatic CSE-model potentials, reflecting the nonuniqueness of the "diabatic" basis. In the case of the *F* and *G* states, the inclusion of nonzero couplings to the *C* state will result in a slight lowering of their fitted diabatic curves. Hence, the corresponding triplet T_e values in Table II may be systematically high when considered against the singlet T_e values, which are not subject to the same problem. That is, the singlet-triplet splittings in the last column of Table II may be slight underestimates.

B. Energies and widths

Computed energies, effective rotational constants, and predissociation widths for the specific $^3\Pi_u(v)$ levels involved in the fitting procedure are shown in columns 5, 8, and 11 of Table I, respectively, compared with the corresponding experimental database values. Overall agreement is excellent with only one discrepancy of more than 3σ,[43] occurring for the $C(v=14)$ level of $^{15}N_2$.[44]

The $C(v=0-5)$ and $C'(v)$ levels, and their mutual perturbations due to the $C\sim C'$ interaction, have been discussed in detail in Ref. 2. CSE-model spectroscopic parameters and predissociation widths for the nominal $C(v=6-20)$ levels of $^{14}N_2$ and $^{15}N_2$ are given in Table III, and those for the nominal $F(v=0-4)$ and $G(v=0-4)$ levels in Table IV.[45] Also shown in the last three columns of Tables III and IV are the computed electronic parentages for the coupled $^3\Pi_u(v)$ levels. For $^{14}N_2$, the $C(v)$ valence levels are relatively pure, with at least 92% *C*-state character. On the other hand, in the case of $^{15}N_2$, there is much stronger mixing with the Rydberg levels, particularly for $C(v=16-17)$. This increased mixing is fortuitous, related to the differential isotopic shifts between the low-*v* Rydberg and high-*v* valence levels leading to closer degeneracies. In the case of the Rydberg states, there is substantial $F\sim G$ mixing, for all vibrational levels, in each isotopomer. Furthermore, there are significant *C*-state admixtures in the Rydberg $v=2-3$ region, especially in the case of $^{15}N_2$, where it is sometimes extremely difficult to determine the principal electronic character of a particular level.

Of particular interest, due to the strong Rydberg–Rydberg mixing, the computed rotational constant for the $F(v=0)$ level of $^{14}N_2$ is 0.071 cm^{-1} higher than that ex-

TABLE III. Computed spectroscopic parameters, predissociation level widths, and electronic parentage for the coupled $C\,^3\Pi_u$ states of $^{14}N_2$ and $^{15}N_2$.

Isotopomer	Level	T_{calc} [a]	B_{calc} [b]	Γ_{calc} [c]	%C	%F	%G
$^{14}N_2$	$C(v=6)$	99 800.7	1.120	1.7	100	0	0
	$C(v=7)$	101 068.9	1.407	15.2	100	0	0
	$C(v=8)$	102 052.3	1.301	17.2	100	0	0
	$C(v=9)$	102 900.8	1.307	83.3	100	0	0
	$C(v=10)$	103 699.	1.33	145.	99	0	1
	$C(v=11)$	104 464.	1.31	145.	99	0	1
	$C(v=12)$	105 241.1	1.26	101.	100	0	0
	$C(v=13)$	106 017.4	1.199	60.4	98	1	1
	$C(v=14)$	106 785.1	1.159	19.2	99	1	0
	$C(v=15)$	107 537.8	1.140	10.8	98	1	1
	$C(v=16)$	108 293.0	1.154	0.01	93	5	2
	$C(v=17)$	109 034.2	1.109	16.5	96	2	2
	$C(v=18)$	109 724.3	1.096	4.0	94	2	4
	$C(v=19)$	110 412.6	1.060	26.7	95	5	0
	$C(v=20)$	111 060.1	1.00	89.	92	3	5
$^{15}N_2$	$C(v=6)$	99 665.6	1.052	0.06	100	0	0
	$C(v=7)$	100 892.5	1.327	12.8	100	0	0
	$C(v=8)$	101 877.	1.27	119.	99	0	1
	$C(v=9)$	102 642.	1.31	169.	96	0	4
	$C(v=10)$	103 389.	1.27	134.	99	0	1
	$C(v=11)$	104 166.6	1.169	60.7	100	0	0
	$C(v=12)$	104 950.4	1.136	18.2	100	0	0
	$C(v=13)$	105 728.0	1.105	1.6	100	0	0
	$C(v=14)$	106 478.3	1.138	0.02	86	10	4
	$C(v=15)$	107 220.2	1.069	11.6	99	0	1
	$C(v=16)$	107 964.	1.23	85.	64	14	22
	$C(v=17)$	108 626.	1.0	197.	57	28	15
	$C(v=18)$	109 342.8	1.021	75.	96	1	3
	$C(v=19)$	109 976.4	0.96	98.	90	8	2
	$C(v=20)$	110 635.6	1.116	0.08	77	12	11

[a] T_{v0} in cm^{-1}.
[b] Effective rotational constant for $J \leq 5$ in cm^{-1}.
[c] Predissociation level width for $J=0$ in cm^{-1} FWHM.

pected for the $v=0$ level of a Rydberg state built on the $A\,^2\Pi_u$ ionic core $[B(A,v=0)=1.735\ cm^{-1}]$,[37] while that for the $G(v=0)$ level is 0.038 cm^{-1} lower than expected for a state built on the $X\,^2\Sigma_g^+$ core $[B(X,v=0)=1.922\ cm^{-1}]$.[37] Sprengers *et al.*[10] performed a two-level analysis of the $F(v=0)\sim G(v=0)$ interaction, deducing a 67%–33% mixing with perturbations in B of $\pm 0.061\ cm^{-1}$. The present results in Table IV show that this simple two-level picture is only an approximation. In fact, a multilevel analysis is required, the 58%–42% and 77%–23% mixings, respectively, for $F(v=0)$ and $G(v=0)$, leading to the significantly unequal corresponding perturbations in B.

A complete picture of the energy and B-value perturbations for the coupled C', C, F, and G states is given in Fig. 3 for the case of $^{14}N_2$, the plotted values representing differences between the computed CSE-model values and the corresponding uncoupled values, the latter determined using the relevant diabatic potentials. For the most part, the C-state perturbations display the classical oscillatory character expected for an outer-limb crossing,[24] reflecting the significant valence-valence interaction with the C' state (see Fig. 2). On the other hand, the large Rydberg–Rydberg interaction is primarily responsible for the extensive energy and B-value perturbations in the F- and G-state levels, which have led to the previous difficulties in their assignments.

The computed CSE-model predissociation level-width patterns for the coupled C, F, and G states of $^{14}N_2$ and $^{15}N_2$ are shown in Fig. 4, in comparison with the few experimental values available. It is no accident that the experimental data are restricted to the levels predicted to be narrower in the calculations: the measurement of broad levels in dipole-forbidden spectra, either directly or indirectly, is very difficult. It is likely that experimental confirmation of the broader $^3\Pi_u$ levels will be provided only indirectly, through their spin-orbit-mediated predissociation of the dipole-accessible $^1\Pi_u$ levels.

Broadly speaking, the width pattern for the C state is oscillatory, with a downward shift for the heavier isotopomer, as expected for the outer crossing by the perturbing and predissociating C' state.[24] However, in the region above $\sim 106\,000\ cm^{-1}$ there are additional sharper width variations caused by the further couplings involving the F and G states, especially in the case of $^{15}N_2$. The width patterns for the strongly coupled F and G Rydberg states display single

TABLE IV. Computed spectroscopic parameters, predissociation level widths, and electronic parentage for the coupled $F\ ^3\Pi_u$ and $G\ ^3\Pi_u$ states of $^{14}N_2$ and $^{15}N_2$.

Isotopomer	Level	T_{calc} [a]	B_{calc} [b]	Γ_{calc} [c]	%C	%F	%G
$^{14}N_2$	$F(v=0)$	104 730.6	1.806	0.46	0	58	42
	$F(v=1)$	106 579.4	1.745	16.2	1	78	21
	$F(v=2)$	108 649.	1.70	148.	10	64	26
	$F(v=3)$	109 972.	1.73	138.	10	45	45
	$F(v=4)$	111 844.5	1.736	17.1	2	56	42
	$G(v=0)$	103 317.4	1.884	0.09	0	23	77
	$G(v=1)$	106 166.8	1.839	9.6	2	27	71
	$G(v=2)$	108 032.0	1.780	89.	6	30	64
	$G(v=3)$	110 831.	1.8	223.	21	38	41
	$G(v=4)$	112 641.0	1.757	37.4	2	46	52
$^{15}N_2$	$F(v=0)$	104 703.9	1.688	0.41	0	57	43
	$F(v=1)$	106 538.0	1.577	16.5	13	68	19
	$F(v=2)$	108 575.7	1.38	73.	45	39	16
	$F(v=3)$	109 776.	1.7	210.	24	36	40
	$F(v=4)$	111 607.3	1.622	42.2	3	55	42
	$G(v=0)$	103 324.3	1.759	0.08	0	23	77
	$G(v=1)$	106 110.6	1.719	8.1	1	29	70
	$G(v=2)$	107 881.3	1.445	23.0	35	21	44
	$G(v=3)$	110 530.	1.6	260.	41	34	25
	$G(v=4)$	112 397.0	1.641	15.4	7	44	49

[a] T_{v0} in cm^{-1}.
[b] Effective rotational constant for $J \leq 5$ in cm^{-1}.
[c] Predissociation level width for $J=0$ in cm^{-1} FWHM.

maxima in the $v=2-3$ region near 110 000 cm^{-1}, caused principally by the direct coupling of these states to the repulsive C' state, which crosses the F state low on the outer limb, in the region of $v=1$. It is not until $v=4$, near 112 000 cm^{-1}, that the Rydberg widths are predicted to decrease significantly. Further experimental data in this region would be invaluable to better constrain the CSE-model parameters. In summary, the $^3\Pi_u$ manifold exhibits a very strong degree of predissociation, with individual vibrational levels predicted to have widths as high as 260 cm^{-1} full-width at half-maximum (FWHM), right across the energy region $>$101 000 cm^{-1}. In the lower part of this region, below $\sim$105 000 cm^{-1}, indirect predissociation via spin-orbit coupling to the C state, itself electronically coupled to the C' state, has been shown to be the driving mechanism for broadening of the $^1\Pi_u$ levels which are accessible in dipole-allowed transitions from the ground state.[2] The present results imply that similar mechanisms are likely to control $^1\Pi_u$-level predissociation at higher energies, at least up to the

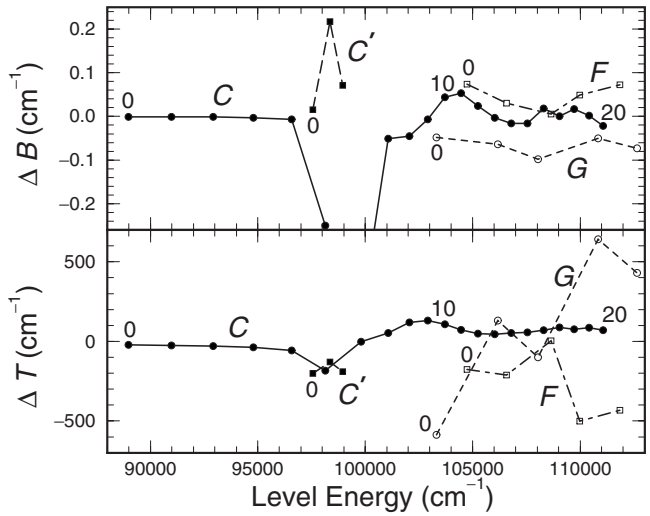

FIG. 3. Computed level shifts ΔT and B-value perturbations ΔB for the $C'\ ^3\Pi_u$, $C\ ^3\Pi_u$, $F\ ^3\Pi_u$, and $G\ ^3\Pi_u$ states of $^{14}N_2$, caused by couplings within the $^3\Pi_u$ manifold.

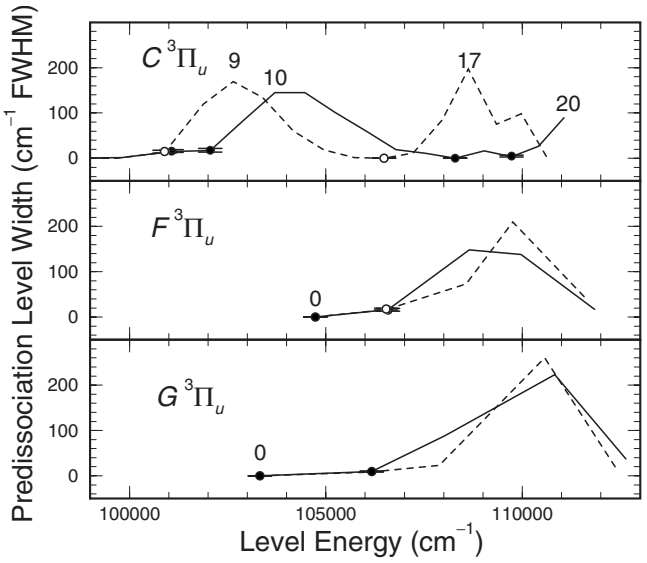

FIG. 4. Computed CSE-model predissociation level-width patterns for the $C\ ^3\Pi_u$, $F\ ^3\Pi_u$, and $G\ ^3\Pi_u$ states of $^{14}N_2$ (solid line vertices) and $^{15}N_2$ (dashed line vertices) compared with the available experimental values from Table I (solid and open circles, respectively).

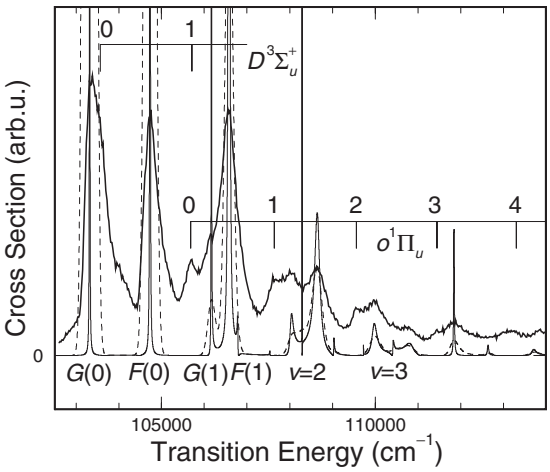

FIG. 5. Comparison between the computed artificial CSE cross section for absorption from the ground state of $^{14}N_2$ into the coupled $^3\Pi_u$ manifold and an experimental KER spectrum following the dissociative charge transfer of an N_2^+ beam in Cs vapor. Thick curve: KER spectrum from Fig. 3 of Ref. 8. Thin solid curve: CSE spectrum for $J=0$, with only the $G\,^3\Pi_u$ state driven. Dashed curve: convolution of CSE spectrum with a Gaussian of 200 cm^{-1} FWHM. Spectral features are labeled according to the relevant excited state except for the $v=2$ and $v=3$ Rydberg vibrational complexes. See text for details.

$\sim$117 000 cm^{-1} dissociation limit of the $b\,^1\Pi_u$ state, but with the indirect dissociation mechanism now also involving the Rydberg F and G states.

C. Cross sections

As mentioned in Sec. II A, since none of the excited $^3\Pi_u$ states considered here is connected to the $X\,^1\Sigma_g^+$ ground state of N_2 by an electric-dipole-allowed transition, it is necessary to artificially define at least one of the diabatic-basis transitions to have a nonzero electronic transition moment in order to obtain a cross section and study the energy structure of the coupled spectrum. In Fig. 5, the computed cross section is shown (thin solid curve) for the transition from $X(v=0,\ J=0)$ of $^{14}N_2$ to the (artificial) $J=0$ level of the coupled $^3\Pi_u$ states, with only the G-X component driven, i.e., the G-X diabatic electronic transition moment is taken as unity, while the others are zero. The most prominent features in this computed spectrum thus correspond to excitation of the Rydberg G and F states, the F-state features occurring only due to intensity borrowing from the G-X transition through the strong $G\sim F$ coupling discussed in Sec. III A. In fact, two of the $F(v)$-$X(0)$ peaks are considerably stronger than the corresponding $G(v)$-$X(0)$ peaks ($v=1,2$), behavior not possible for simple $\Delta v=0$ two-level mixing, confirming the multilevel nature of the Rydberg-state mixing. The strong perturbation and predissociation associated with the mixed Rydberg states produce an interesting spectral structure. While the $G(v=0)$ and $F(v=0)$ peaks are well separated, the $v\geq 1$ peaks tend to cluster together in "vibrational complexes." In the case of the $v=2$ and 3 complexes (so labeled in Fig. 5), the peak widths are comparable with their separations, leading to quantum-interference effects and a structured-continuum appearance. In addition, the $C(v=16)$ and $C(v=19)$ valence levels (narrower computed peaks in Fig. 5) are embedded in the $v=2$ and 3 complexes, respectively.

The CSE spectrum provides a convincing means to interpret the kinetic-energy-release (KER) spectra of van der Kamp *et al.*,[8] obtained following the dissociative-charge-transfer neutralization of a high-energy N_2^+ beam in Cs vapor. The KER spectrum from Fig. 3 of Ref. 8 is also shown in Fig. 5, recalibrated in terms of the excited-state energy using the accurately known energies of the $G(v=0)$, $F(v=0)$, and $o(v=0-3)$ levels. At the lower energies, the $G(v=0)$, $F(v=0)$, and $D\,^3\Sigma_u^+(v=0,1)$ levels are associated with prominent KER features, while the $o(v)$ progression used for calibration appears weakly across the whole energy range. By comparison with the computed CSE spectrum, degraded to account for a finite instrumental resolving power (dashed curve in Fig. 5), it is apparent that most of the KER spectrum is associated with the excitation of the Rydberg $^3\Pi_u$ manifold. In particular, the $G(v=1)$ peak appears as a shoulder on the left-hand side of the much stronger $F(v=1)$ peak, and the Rydberg $v=2$ and 3 complexes appear clearly. There is even a very weak inflection in the KER spectrum, within the $v=3$ complex, which appears at the predicted energy of the $C(v=19)$ level. By employing laser excitation of the reactant ion beam, van der Kamp *et al.*[8] obtained difference KER spectra characteristic of the excitation of specific vibrational levels of Rydberg states built on the $A\,^2\Pi_u$ ion core. In the $v=2$ case, they reported an unusually broad $F(v=2)$ feature, attributed to an unresolved overlapping peak. The CSE spectrum clearly shows that the overlapping feature is due to $G(v=2)$ [together with a little $C(v=16)$], i.e., the broad feature is, in fact, the $v=2$ Rydberg complex. Thus, overall, comparison with the CSE spectrum shows that it is possible to understand the unidentified KER peaks of Ref. 8, the present work providing the first correct assignment of the $G(v>0)$ levels.

We caution that the CSE-KER comparison is not intended to be quantitative with respect to relative vibrational intensities since the KER spectrum arises from the ionic ground and excited states, while the CSE spectrum involves excitation from the ground state of N_2. Furthermore, the KER spectrum is uncorrected for detector sensitivity effects. Nevertheless, it is clear that the strong $F\sim G$ coupling will always result in the appearance of both F- and G-state features in any type of spectrum, with non-Franck–Condon intensities, *regardless* of whether only one or both of these states are driven in the particular excitation process.

It has been pointed out in Sec. III A that the CSE model is not expected to be valid in the energy region above the $v=3$ complex. In Fig. 5, it can be seen that, while the calculated $F(v=4)$ peak near 112 000 cm^{-1} coincides with a peak in the KER spectrum, at higher energies there is no correspondence between the two spectra. If the KER peaks in this energy range are due to the excitation of $^3\Pi_u$ levels, as is quite likely, then it will clearly be necessary to add further basis states to the current model in order to become quantitative in this region.

IV. SUMMARY AND CONCLUSIONS

New and existing spectroscopic data on N_2, obtained using a wide variety of experimental techniques, have been interpreted using a CSE model of the structure and predissociation dynamics for the interacting Rydberg and valence states of $^3\Pi_u$ symmetry. A four-channel CSE model, which includes the $F\ ^3\Pi_u$ and $G\ ^3\Pi_u$ Rydberg states and the $C'\ ^3\Pi_u$ and $C\ ^3\Pi_u$ valence states, indicates strong Rydberg–Rydberg coupling between the F and G states, strong Rydberg-valence coupling between the G and C' states, weaker coupling between the F and C' states, and confirms the already-known valence-valence coupling between the C and C' states.

Strong perturbations and predissociations have been identified for most levels in the $^3\Pi_u$ manifold above $\sim 100\,000\ \text{cm}^{-1}$, and the $v>0$ levels of the $G\ ^3\Pi_u$ state have been assigned correctly for the first time. The strong predissociation of the F and G states by the C' state suggests the need to consider these Rydberg states and their interactions, including spin-orbit, in any realistic model of N_2 singlet-state predissociation above a transition energy of $\sim 105\,000\ \text{cm}^{-1}$. There is a need for new *ab initio* calculations of the $^3\Pi_u$ manifold, including a balanced treatment of the Rydberg and valence states, in order not only to confirm the present results, but also to shed some light on the $C\sim F$ and $C\sim G$ electrostatic interactions, which are not obtainable from this study.

ACKNOWLEDGMENTS

This work was supported by Australian Research Council Discovery Program Grants DP0558962 and DP0773050. The authors also thank Dr. Phil Cosby for the provision of a digital version of the spectrum in Fig. 3 of Ref. 8. One of the authors (H.L.B.) thanks the Australian National University for two Visiting Fellowship appointments during the course of this work.

[1] M.-C. Liang, A. N. Heays, B. R. Lewis, S. T. Gibson, and Y. L. Yung, Astrophys. J. **664**, L115 (2007).
[2] B. R. Lewis, S. T. Gibson, W. Zhang, H. Lefebvre-Brion, and J.-M. Robbe, J. Chem. Phys. **122**, 144302 (2005).
[3] G. Joyez, R. I. Hall, J. Reinhardt, and J. Mazeau, J. Electron Spectrosc. Relat. Phenom. **2**, 183 (1973).
[4] J. Mazeau, R. I. Hall, G. Joyez, M. Landau, and J. Reinhardt, J. Phys. B **6**, 873 (1973).
[5] A. Chutjian, D. C. Cartwright, and S. Trajmar, Phys. Rev. A **16**, 1052 (1977).
[6] P. Hammond, G. C. King, J. Jureta, and F. H. Read, J. Phys. B **20**, 4255 (1987).
[7] M. Furlan, M.-J. Hubin-Franskin, J. Delwiche, and J. E. Collin, J. Phys. B **23**, 3023 (1990).
[8] A. B. van der Kamp, P. C. Cosby, and W. J. van der Zande, Chem. Phys. **184**, 319 (1994).
[9] B. R. Lewis, K. G. H. Baldwin, J. P. Sprengers, W. Ubachs, G. Stark, and K. Yoshino, J. Chem. Phys. **129**, 164305 (2008).
[10] J. P. Sprengers, E. Reinhold, W. Ubachs, K. G. H. Baldwin, and B. R. Lewis, J. Chem. Phys. **123**, 144315 (2005).
[11] T. Hashimoto and H. Kanamori, J. Mol. Spectrosc. **235**, 104 (2006).
[12] S. L. Guberman, Geophys. Res. Lett. **18**, 1051 (1991).
[13] C. E. Dateo, personal communication (November, 2004).
[14] H. Partridge, personal communication (March, 1998).
[15] See also: H. Ndome, M. Hochlaf, B. R. Lewis, A. N. Heays, S. T. Gibson, and H. Lefebvre-Brion, J. Chem. Phys. **129**, 164307 (2008).
[16] D. Spelsberg and W. Meyer, J. Chem. Phys. **115**, 6438 (2001).
[17] E. F. van Dishoeck, M. C. van Hemert, A. C. Allison, and A. Dalgarno, J. Chem. Phys. **81**, 5709 (1984).
[18] B. R. Lewis, S. S. Banerjee, and S. T. Gibson, J. Chem. Phys. **102**, 6631 (1995).
[19] In order to study the energy structure of the coupled excited states in this electric-dipole-forbidden transition using the CSE method, we must assume a nonzero electronic transition moment for at least one of the diabatic-basis transitions. In this sense, the photodissociation cross section is artificial.
[20] C. A. Nicolaides and D. R. Beck, Phys. Lett. A **65**, 11 (1978); B. Simon, *ibid.* **71**, 211 (1979).
[21] R. Lefebvre, J. Chem. Phys. **92**, 2869 (1990); Phys. Rev. A **46**, 6071 (1992).
[22] P. K. Carroll and R. S. Mulliken, J. Chem. Phys. **43**, 2170 (1965).
[23] K. Dressler, Can. J. Phys. **47**, 547 (1969).
[24] H. Lefebvre-Brion and R. W. Field, *The Spectra and Dynamics of Diatomic Molecules* (Elsevier, Amsterdam, 2004), pp. 307–315, 399–400, 509–519.
[25] D. Stahel, M. Leoni, and K. Dressler, J. Chem. Phys. **79**, 2541 (1983).
[26] G. H. Dieke and D. F. Heath, Johns Hopkins Spectroscopic Report No. 17, 1959.
[27] S. G. Tilford, J. T. Vanderslice, and P. G. Wilkinson, Astrophys. J. **142**, 1203 (1965).
[28] F. Roux, F. Michaud, and M. Vervloet, J. Mol. Spectrosc. **158**, 270 (1993); Can. J. Phys. **67**, 143 (1989).
[29] J. W. Ledbetter, Jr., J. Chem. Phys. **67**, 3400 (1977).
[30] P. K. Carroll, Proc. R. Soc. London, Ser. A **272**, 270 (1962).
[31] J. W. Ledbetter, Jr. and K. Dressler, J. Mol. Spectrosc. **63**, 370 (1976).
[32] Y. Tanaka and A. S. Jursa, J. Opt. Soc. Am. **51**, 1239 (1961).
[33] The energies for $F(v=2,3)$ and $G(v=2,3)$ were deduced from the KER spectra of Ref. 8, locally recalibrated using the well-known $o(v)$ peaks in the same spectra. As discussed in more detail in Ref. 9, this technique yields more accurate state energies, with lower uncertainties, than those published in Ref. 8.
[34] J. M. Brown and A. J. Merer, J. Mol. Spectrosc. **74**, 488 (1979).
[35] Digital representations of the diabatic potential-energy curves are available from the authors.
[36] The electrostatic interaction matrix element V_{rv} between a valence state v and a Rydberg-series member r, of principal quantum number n, is related to the electron-capture width $\Gamma(R)$, relevant to the dissociative recombination of the ionic state to which the Rydberg series converges, through the relation $\Gamma(R)=\pi(n^*)^3|V_{rv}(R)|^2/\Re$, where $n^*=n-a$, a is the quantum defect, and $\Re$ is the appropriate mass-adjusted Rydberg constant. In the case of the $3p\pi_u G_3\ ^3\Pi_u$ state, $n^*=2.25$.
[37] K. P. Huber and G. Herzberg, *Molecular Spectra and Molecular Structure IV. Constants of Diatomic Molecules* (Van Nostrand, New York, 1979), p. 426.
[38] H. Lefebvre-Brion and C. M. Moser, J. Chem. Phys. **43**, 1394 (1965).
[39] P. Cremaschi, A. Chattopadhyay, P. V. Madhavan, and J. L. Whitten, Chem. Phys. **109**, 117 (1986).
[40] This value represents half of the minimum splitting in the avoided-crossing region between the *ab initio* C- and C'-state potential-energy curves calculated by Robbe and presented in Ref. 2.
[41] This conclusion assumes that additional direct interactions with dissociative valence states do not play a significant role in the predissociation of $G(v=0)$. The *ab initio* calculations of H. H. Michels, Adv. Chem. Phys. **45**, 225 (1981), do not indicate any candidate perturbers, and, in any case, such interactions, which involve the spin-orbit predissociation of a Rydberg state by a valence state, are likely to be weak.
[42] S. L. Guberman, in *Dissociative Recombination of Molecular Ions with Electrons*, edited by S. L. Guberman (Kluwer/Plenum, New York, 2003), p. 192.
[43] For the most precise of the experimental energies and rotational constants in Table I, for which no uncertainties are given, discrepancies of a few tenths and thousandths of a cm^{-1}, respectively, are regarded as satisfactory.
[44] There are three probable contributions to the discrepancies in the energy and rotational constant for $C(v=14)$ of $^{15}N_2$. First, although the experimental rotational data for this level are relatively precise, they are very few, with the full triplet structure not well sampled, leading, perhaps, to optimistic uncertainty estimates in Ref. 9. Second, because of a close perturbation from above by the $F(v=1)$ level, evidenced by the significant centrifugal-distortion constants in Table IV of Ref. 9, the $^3\Pi_u$ Hamil-

tonian (Ref. 34) used to analyze the experimental data may not have been fully applicable. For this reason, we have increased the uncertainty in the experimental $C(v=14)$ rotational constant in Table I. Third, the CSE model employed treats only the $\Omega=1$ components of the $^3\Pi_u$ states, and is thus incapable of representing the J-dependent perturbations caused by the $\Omega=0$ and 2 sublevels of the nearby $F(v=1)$ level.

[45] The spectroscopic parameters listed in Tables III and IV have been deduced using a combination of the two coupled-channel methods discussed in Sec. II. The tabulated energies represent the resonance centers, rather than peaks, this distinction necessary in the case of broader, asymmetric resonances. In a few cases, i.e., for $^{15}N_2$, $C(v=16,17)$, $F(v=3)$, and $G(v=3)$, there are strong interference effects between nearly degenerate broad resonances which limit the precision of the associated spectroscopic parameters. For these levels, the two computational methods yield energies that differ by 5%–15% of the corresponding resonance widths.